Gowree, E.R., Atkin, C.J. & Gruppetta, S. (2015). A simple digital-optical system to improve accuracy of hot-wire measurements. MEASUREMENT SCIENCE and TECHNOLOGY, 26(9),

CITY UNIVERSITY LONDON
EST 1894

City Research Online

A simple digital-optical system to improve accuracy of hot-wire measurements

E R Gowree[1], C J Atkin[2] and S Gruppetta[3]

School of Engineering and Mathematical Science[1,2] and Department of Optometry and Visual Science[3], City University London, Northampton Square, EC1V 0HB, London, UK

Email: erwin.gowree.1@city.ac.uk

Abstract

A high precision traverse mechanism with micro-resolution was designed to capture accurately the velocity profile of the very thin turbulent attachment line on a swept body. To ensure that the traverse mechanism could position the hot wire reliably, a simple digital optical system was designed to check the performance of the traverse by measuring the displacement of the hot wire: a vertical displacement of 2.4µm was achievable and this could be further reduced to 0.6µm using micro-stepping. Due to the simplicity of the set-up it was equally useful for probe wall positioning and the velocity profiles captured clearly demonstrated that the optical set-up helped in resolving the near wall flow more accurately, regardless of the thinness of the boundary layer. The captured data compare well with the results from similar investigations, with arguably higher precision achieved.

Keywords: optical, hot wire, probe wall position

1. Introduction

Coupled with several other advantages the Hot-Wire Anemometry (HWA) technique has gained extensive recognition as being a reliable method for capturing the velocity profiles of boundary layers with minimal intrusive effects due to its microscopic size. Nevertheless, this particular characteristic of the probe can be a hindrance when measuring the position of the probe relative to the wall which is extremely important for accurate resolution of the integral boundary layer properties such as momentum and displacement thicknesses. This is especially true in the case of turbulent boundary layers which tend to exhibit extreme velocity gradients near the wall. Apart from the probe wall position, it is also important to ensure that positions and orientations of the wire supports (Figure 1 below) are known relative to the local velocity vector or else spurious measurements can be obtained due to unaccounted tangential or binormal velocity components.
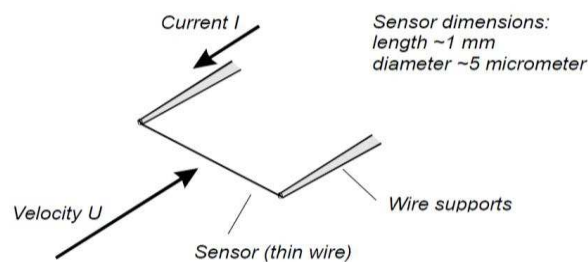
Figure 1: Schematic of the hot wire probe, Bruun [2]

In the early 1960's the issue of probe wall position was addressed by Wills [1] by measuring the distance between the real image of the wire and its reflection using a 45º mirror and microscope with a graduated eye-piece, an accuracy of ±1.27 µm being claimed by the latter. According to Bruun [2] a similar approach was adopted by Van Thinh [3], Krishnamoorthy et al. [4] and Devenport et al. [5] later. However even with the high accuracy achievable with this method there can be drawbacks, for example in cases where the reflected image is not of a good quality due to distortion, or even unavailable due to the surface finish of the wall. The method is also not appropriate for measurements above curved surfaces. A different method employed by Orlando [6]

consisted of a mechanical stop with a known reference height placed on the wall and when the wire was brought in contact with the stop, which was confirmed optically the reference height was taken as the probe wall position. Using this method an accuracy of ±25µm was obtained which is rather low for the measurement of thin boundary layers of the orders of 1 or 2mm. Hutchins and Choi [7] explored the method employed by Kerho [8]: in this case one of the wire supports connecting the hot wire was brought in contact to an electrically conductive film which was sprayed on the wall of the model. Upon contact with the live conductive film the circuit was closed and the wire support was assumed to be touching the surface. From this method an accuracy of ±25µm was achievable and according to Hutchins and Choi this accuracy could have been be improved if a traverse with finer resolution were available.

The benefit of laser and optical fibre technology was recognized by Takagi [9], who designed a system consisting of an emitter generating a laser beam parallel to the surface of the model and a photodiode receiver made up of an array of optical fibres to detect the laser beam at the opposite end. The interference introduced in the laser beam from the bottom of the wire support when it was shifted closer to the wall could be detected by the receiving optics and hence the position of the hot-wire sensor with an accuracy of ±10 µm. Hutchins and Choi also employed lasers and used the triangulation principle. A module containing both the laser diode and the receiving optics was fixed parallel to the probe support at a known perpendicular distance between the sensor wire and a given point on the model. Then using an accurate traverse mechanism the probe was displaced closer to the wall and the position was estimated using the reference length and the height travelled during the traverse. Using this method Hutchins and Choi claimed that an accuracy of ±5µm was achievable.

The viscous flow at the leading of swept wings is highly complicated due to the three dimensional nature of the boundary layer in the presence of highly curved streamlines. The present work was aimed at extending the knowledge on the attachment line (AL) boundary layer and the neighbouring flow by capturing the velocity profiles both in the laminar and turbulent state using constant temperature HWA. Studies of the turbulent AL are limited to the experimental investigations of Gaster [10], Cumpsty and Head [11] conducted in the late 1960s and more recently in 2013 by Atkin and Gowree [12]. The boundary layer on a wing (or body) is at its thinnest at the AL so a traverse gear with very fine resolution is needed to capture the profiles accurately. The curvature of the wing surface is also at a maximum near the AL (at the leading edge), therefore an accurate alignment method was required.

The main purpose of this paper is to present the capabilities and limitations of a digital-optical probe alignment system designed to check the performance and accuracy of such traverse mechanism, in particular during measurement of the probe wall position, which is crucial for capturing the velocity profile. The physics of the AL will not be covered in great detail but it is worth introducing the basics. In simple terms, if a wing of high aspect ratio (ratio of span to mean geometric chord) is considered as a series of two-dimensional aerofoil sections, the AL is an imaginary line that progresses in the spanwise direction connecting all the points of attachment of the constituent aerofoil sections. For a swept wing, the non-zero component of flight velocity along the span of the wing gives rise to a viscous flow known as the AL boundary layer which is also the origin of the boundary layer developed over the rest of the wing. From the studies conducted by Pfenninger [13], Gaster [10] and Poll [14] the AL can be characterised by the Reynolds number,

$$R_\theta = \frac{V_e \theta_{11}}{v_\infty} \quad or \quad \bar{R} = \frac{V_e \eta}{v_\infty}$$

(1)

where η is a viscous length scale given by

$$\eta = \left(\frac{v_\infty}{\left[\frac{dU_e}{dx} \right]_{x_\infty}} \right)^{\frac{1}{2}}$$

V_e and U_e are the spanwise and chordwise velocity components respectively (see figure 2), at the edge of the boundary layer at the point of attachment, θ_{11} is the streamwise momentum thickness and v_∞ the freestream

kinematic viscosity. By solving the governing boundary layer equations representing 'Swept Hiemenz Flow', from Rosenhead [15], for a laminar AL

$$R_\theta = 0.4042\bar{\bar{R}}$$

(2)

$$\theta_{11} = \int_{z=0}^{z=\delta} \frac{v}{V_e}\left(1 - \frac{v}{V_e}\right) dz$$

where z is the direction normal to the surface.

A criterion for the susceptibility of the attachment line to contamination from a turbulent boundary layer occurring from a side body, such as a fuselage or wind tunnel wall, was established by Pfenninger, Gaster and later confirmed by Poll. According to the latter the contamination spreads along an AL and the rest of the boundary layer over a wing once the Reynolds number exceeds a critical value: $\bar{R} > 250$ or $R_\theta > 100$.

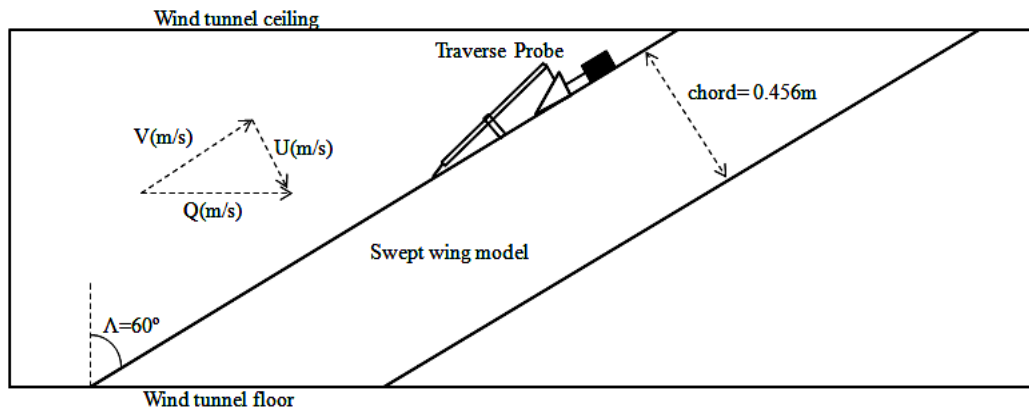## 2. Experiment
2.1. Wind tunnel model

Figure 2: Side view of the swept NACA0050 model inside the test section of the T2 wind tunnel.

A wooden experimental model was designed in such a way that attachment line $\bar{R} \approx 500$ could be attained while running the tunnel at 45 m/s. This is about the 80% of the achievable wind speed in the empty test section (1.8m×1.12m×0.8m) of the T2 wind tunnel at the Handley Page laboratory at City University London. For this freestream velocity and a sweep angle of 60°, a leading edge radius of curvature of 0.114m was required. A NACA0050 aerofoil with a normal to leading edge chord length of 0.456m was chosen in preference to a cruder model employing a circular cylinder section faired to a tear-drop, as employed by Gaster, Cumpsty and Head and Poll, in order to avoid separation at the shoulder where the thickness is at its maximum, and the surface curvature discontinuous, and hence to reduce the blockage caused by the wake of the model. More information about the design of the experimental model can be obtained from Atkin and Gowree [16]. Figure 2 shows the model mounted between the floor and the ceiling of the T2 test section, where the turbulent boundary layer from the tunnel floor was used as a source of contamination to generate a turbulent AL at and above the critical $\bar{R}$ value.

2.2. Boundary Layer Traverse Mechanism

To hold the HWA probe a surface mounted traverse mechanism shown in figure 3 was designed and manufactured in-house. The traverse is driven by the Nanotec GmbH & Co LS2018S0604 linear actuator, which consists of a ST2018 stepper motor and TR6×2 translation screw with a range of 50mm. The stepper motor has an angular resolution of 1.8 degrees per step or a linear resolution of 10μm per step in the linear actuator mode, with an accuracy of ±5% per step due to backlash and errors from the electronic components, which is nevertheless non-accumulative for a stepper movement consisting of multiple steps. Micro-stepping can be

achieved to a ratio of 1/64 using the SMCI12 controller which was supplied by Nanotec. The linear actuator can be operated from a PC via NanoPro software, also supplied by Nanotec.
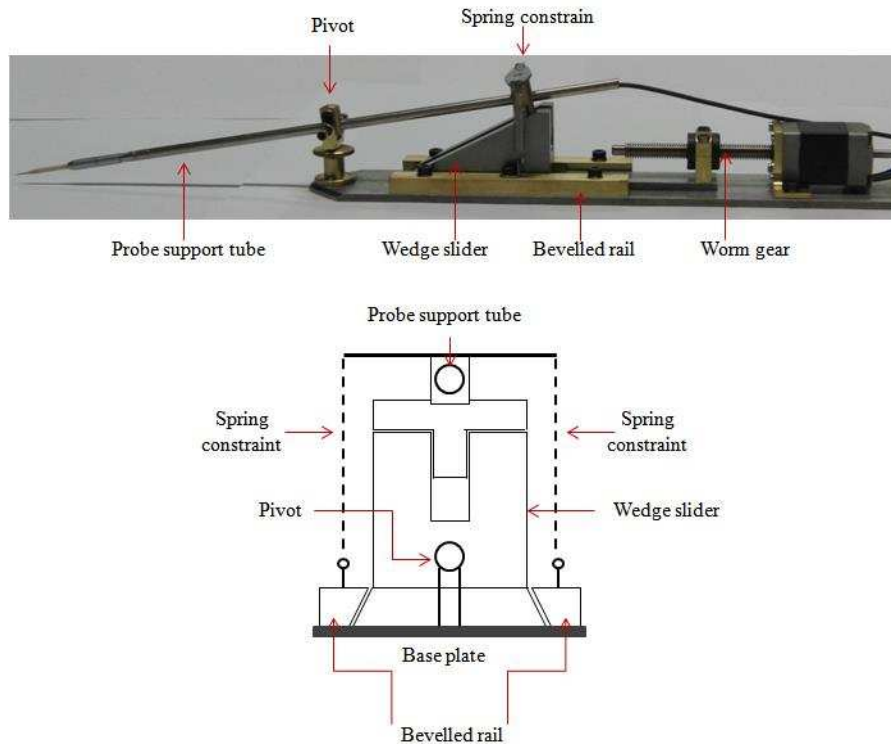

Figure 3: Side view of traverse gear (top) and a schematic representation of elevation view (bottom).

As shown in figure 3, as the linear actuator pulls the sliding wedge horizontally towards the right hand side (RHS), the hot-wire probe pitches up, away from the wall; and vice versa. The tangent of the wedge angle is 0.5: a further gearing can be obtained by adjusting the probe holder so that the arm on the left hand side (LHS) of the pivot is half the length of the RHS. In this way the ratio between the linear displacements by the actuator and the resulting vertical pitch of the probe can be reduced by a factor of 4. With this gearing, a probe motion of 2.5μm per step is anticipated, which is half the diameter of the hot-wire probe and therefore sufficient for the current study. The SMCI12 controller possesses built-in micro-stepping capabilities up to a ratio of 1/64 (finest resolution of 0.028 degrees per step) and therefore a further reduction can be achieved. However, the accuracy of the measurement will be severely compromised for such a small stepper motor and the manufacturer recommended a micro-stepping limit of ¼ for acceptable accuracy. Micro-stepping was not applied during the boundary layer traverse in the current experiment but was used for near-wall alignment, during which process the accuracy was verified (see section 3.1).

2.3. Hot Wire Set-up and Calibration
A Dantec 55P15 hot-wire probe was connected to a DISA 55M10 CTA Standard Bridge module (which consists of a Wheatstone bridge with an integrated servo). This was interfaced with the National Instruments (NI) DAQ card for data acquisition and processing in NI-Labview. During the boundary layer measurement the sampling rate in Labview was set at 100 kHz (mainly for the purposes of a companion experiment investigating laminar-turbulent transition, with a need to capture turbulent frequencies of approximately 30 kHz) and the overheat ratio of the CTA module was adjusted to a value of 2.0. Initial measurements and spectrum analysis suggested that the mean-flow measurements needed pre-filtering prior to acquisition and a 5 kHz R-C filter was employed. The sampling rate was not reduced as over-sampling was not thought to introduce any form of error nor impair the measurements. King's Law [17] with the linearised correlation was preferred for the calibration; however, due to temperature drift during the tunnel runs, the method for temperature correction given by equation 4, initially formulated by Collis and Williams [18] and later modified by Abdel-Rahman et al. [19] was employed for the correction of errors introduced by temperature drift.

$$Nu \left(\frac{T_m}{T_a}\right)^a = A + B\,Re^n \tag{3}$$

Here T_a represents the freestream ambient temperature and T_m the average between the sensor temperature, T_s and the ambient temperature; the powers a and n are equal to -0.17 and 0.45 respectively. The Nusselt number, Nu, and the Reynolds number, Re, based on the hot-wire sensor characteristic length and resistance can be expressed as

$$Nu = \frac{E^2}{R_s \pi l k (T_s - T_a)} \quad , \quad Re = \frac{ud}{v}$$

R_s and d represent the resistance and diameter of the sensor respectively and u the local velocity at the sensor. The thermal conductivity, k, and kinematic viscosity, v, can be estimated using the relations below, based on the mean temperature between the sensor and the ambient fluid.

$$\frac{k}{k_a} = \left(\frac{T}{T_a}\right)^{0.86} , \qquad \frac{v}{v_a} = \left(\frac{T}{T_a}\right)^{1.9}$$

The thermal conductivity of the ambient fluid, k_a can be estimated using Kannuluik and Carman's relation quoted by Collis and William [18] and given by equation 4, where the units of k_a are W / (cm K) and the viscosity can be estimated using Sutherland's law.

$$k_a = 2.41 \times 10^{-4}(1 + 0.00317\,T - 0.0000021\,T^2) \tag{4}$$

Calibration was undertaken by mounting the probe parallel to the axis of the wind tunnel with the hot wire normal to the freestream air. A Pitot-Static probe was mounted close enough and parallel to the hot-wire support, while ensuring that no flow interference was introduced by either device. The air speed measurement was obtained using the Furness Control FC0318 differential pressure transducer which was sent for factory recalibration and checked using a water column differential pressure manometer (distilled water) with an accuracy of 0.01 mm H$_2$O. The output from the pressure transducer was connected to a NI-Labview module and was converted into speed using the factory calibration. This enabled the hot-wire voltage output to be recorded simultaneously with air speed during the calibration process. By plotting the term on the LHS of equation 3 with respect to Re^n computed from the calibration data, the values of A and B were determined and used for further data reduction during the measurement of the velocity profile.

2.4. Optical System Set-up

The optical alignment system included back illumination of the hot wire probe (white light LED illuminator LIU004, Thorlabs Ltd) and a pair of identical achromatic doublet lenses (Linos Photonics AC254-100-A-ML, focal length f=100mm). The set-up is illustrated schematically in figure 4. The image of the hot wire was captured using a CCD camera (QImaging Rolera). The set-up could be configured for different magnification settings by varying the ratio of the image distance (distance of image formed on CCD camera from the lens pair) to object distance (distance of hot-wire probe from lens pair). The measurements presented in this paper were taken with magnifications ranging from 9× to 20×.
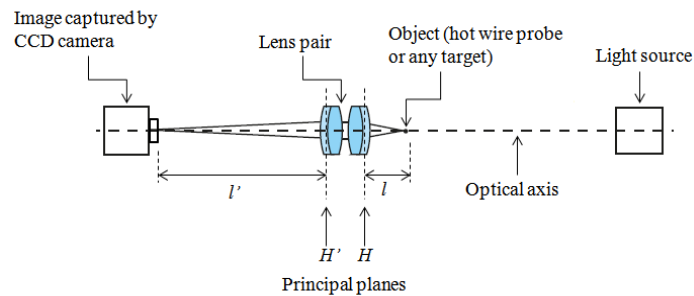

Figure 4: Optical arrangement to represent the magnification process.

From Jenkins and White [20], the path of a ray of light emerging from a medium and passing through a spherical surface can be represented by the relation given by

$$\frac{n}{l} + \frac{n'}{l'} = \frac{n' - n}{r}$$

(5)

where l represents the distance from the object and the principle plane, l' the distance between principle plane and the image, and r, the focal length. If the light path passes through two different media then n would be the refractive index of the medium in which the object lies and n' the refractive index of the medium where the image is located. See `FIGURE 3K' and `pp. 56' from reference [20] for more details about the derivation.

If the ray of light is travelling through a thin lens and the same medium, which would be air for the current application, the power of that lens can be expressed as

$$\frac{1}{l} + \frac{1}{l'} = \frac{1}{f}$$

(6)

Based on the optical system in figure 4, f denotes the focal length of the lens and l represents the distance between the object and the primary principle plane H, and l' the distance between the secondary principle plane H' and the image in focus. By simplifying the lens formula the magnification can be expressed as

$$M = \frac{1}{l'}$$

(7)

Prior to utilisation, the optical system was calibrated by placing a reference target at the object plane instead of the hot-wire probe. The reference targets used were either a USAF resolution target (black on clear glass used in transmission, Edmund Optics) or the inner spacing between the jaws of a digital calliper. These targets of known dimensions enabled the calibration of the image obtained with the CCD camera using the following procedure. The jaws of the digital calliper were set at 300 ±10 µm, placed in front of the lens and translated back and forth to bring into focus, so that this calibration gauge was located exactly at the object plane. Figure 5(a) shows the image obtained, where the lighter region shows the gap in between the jaws of the calliper and the black patches on the sides represents the jaws. By plotting the colour intensity along a reference horizontal cross-section, y = 200 pixels as shown in figure 5b (red dashed line in figure 5a), the edges of the calliper jaws was represented by the darkest parts of figure 5a and were assigned with the minimum value (intensity = 0) and the peaks represented the gap between the jaws (intensity > 0). The number of pixels (505) representing the grey region was obtained after 'binarising' the plot as shown in figure 5c. From the 'binarised' image the pixel count (with an accuracy of ±2 pixels) representing a length of 300 µm ±10 µm can be obtained, therefore providing a conversion factor between pixels on the CCD and object plane coordinates. The CCD camera used had square pixels and therefore the calibration is identical in both horizontal and vertical directions. Based on the accuracy of the digital calliper and the accuracy in binarisation, the resolution of 1 pixel was determined to be 0.59 µm within ±0.036µm.
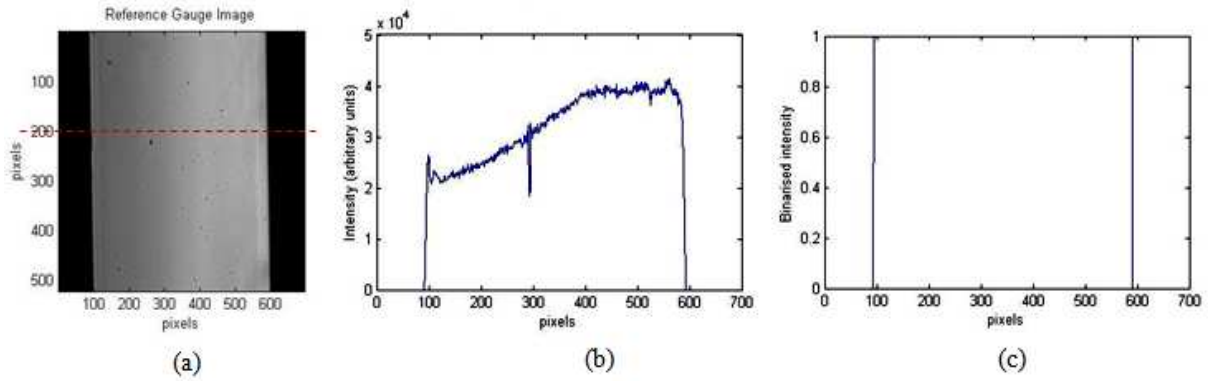
Figure 5: (a) Image of the 300µm jaw spacing in a Vernier calliper, (b), Corresponding intensity cross-section along the horizontal reference axis y=200 pixels given by the dashed red line in 5(a), (c), intensity cross-section binarised at 1×10^4.

3. Results and Discussion

3.1. Calibrating and Commissioning the Traverse Mechanism

By applying the procedures outlined above, the vertical displacement of the hot-wire probe generated by the traverse mechanism can be measured by comparing the images of a reference position and final displaced position. Figure 6 shows a magnified snap shot of the initial position (reference position) of the hot wire and the tip of the probe support, and the position after one step of the stepper motor. The dark patch on the bottom right corner is the side of the adjacent probe support which was out of focus. A cross-section of the image along the vertical direction (averaged over the range $100 \leq x \leq 200$ pixels) is plotted in figure 7, showing the pixel intensity values at both positions. By comparing these figures, one can see that the minimum point on the trough of the intensity plots, which represents the centre of the hot wire, has shifted by a very small amount along the x-axis and this represents the displacement of the probe in pixels. Using the method of converting pixel to a physical length established above, it is possible to measure the displacement brought about by a full-step motion. A displacement of $2.41 \pm 0.09 \mu m$ was determined for this particular case. Measuring the displacement brought about by a number of successive full-step motions increases the accuracy of the calculation.

In order to measure finer displacements the magnification of the optical set-up has to be increased. However, in doing, so the image becomes blurred, owing to an increase in optical aberrations, and the accuracy is compromised. Instead of measuring the displacement for every single step, the displacement of a range of steps can be measured and the mean of that sample can be derived. Therefore, using this particular technique the minimum displacement achievable by the traverse gear was estimated to be approximately $0.60 \pm 0.02 \ \mu m$ for a quarter-step motion generated by the stepper motor, using the micro-stepping function available from the controller. According to the manufacturer's specification, for this particular step-size a displacement of 0.625 μm is expected, so a measured displacement of $0.60 \pm 0.02 \ \mu m$ demonstrates acceptable accuracy for ¼ step micro-stepping.
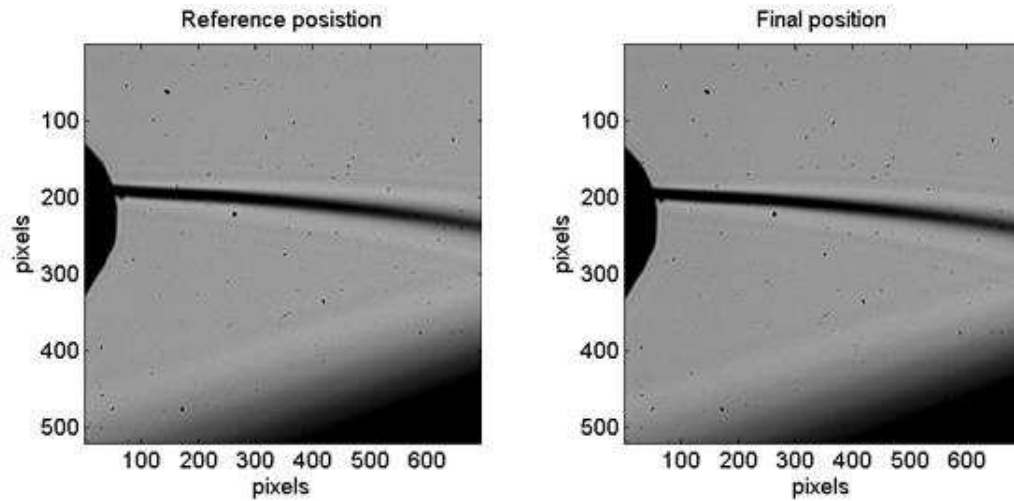
Figure 6: Optical image of the hot wire before (LHS) and after (RHS) 1 step.

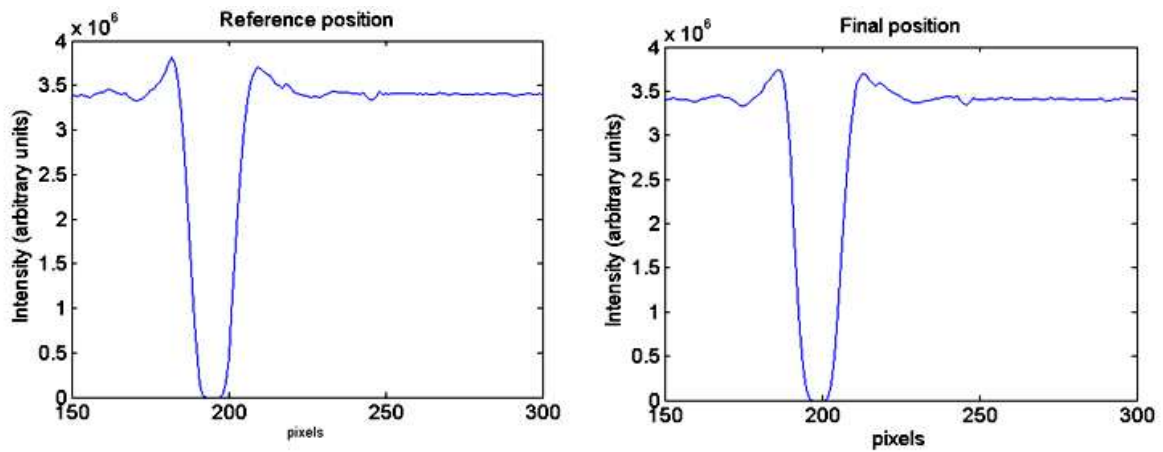Figure 7: The vertical cross-section intensity trace at 100 pixels and the trace after 1 motor-step.
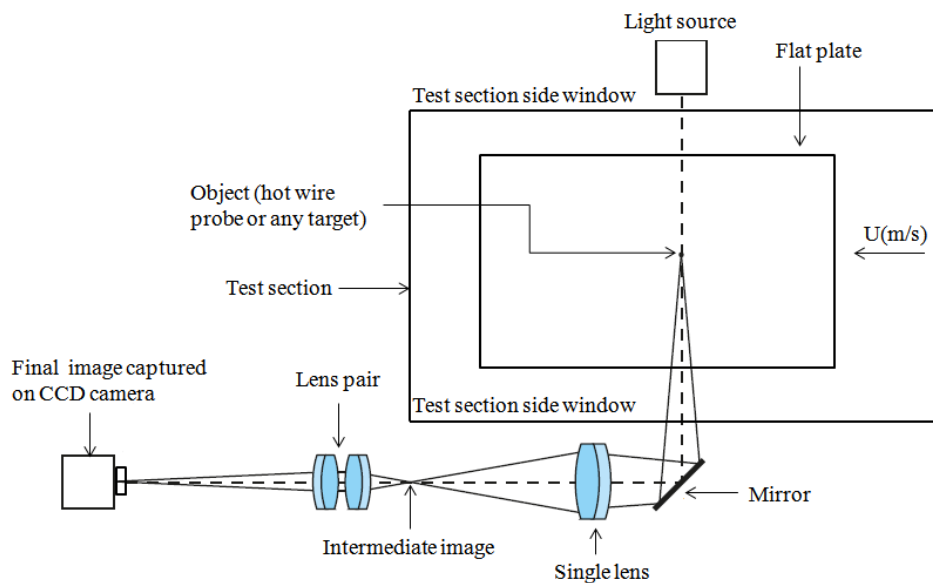
3.2. Aligning the Hot-wire Probe

Figure 8: Schematic representation of the top-view of the optical set-up used for near wall probe alignment on the flat model where the optics are kept outside the test section.

A first attempt to apply the technique in situ in the test section of the wind tunnel involved positioning the optical system outside the test section, using a two-step magnification phase shown figure 8. The optical principle here is similar to that applied above, except the introduction of the single lens as an intermediate stage. From equation 9, for a lens with a given focal length the magnification is inversely proportional to the distance between the object and the primary principle plane, l. In order to keep the optics outside the test section this minimum distance needed to be approximately 60cm, which is half the width of the working section, plus the thickness of the side window, plus a certain amount of clearance for an object located at the middle of the test section. Therefore, for a magnification of at least 10×, a bigger lens would be required with a longer focal length, resulting in quite a large distance between the secondary plane and image in focus. This was avoided by inserting the intermediate lens and its image could be used as the object for the second doublet lens which served as the magnifier. The feasibility of the new set-up (with the optics mounted outside the test section) was tested by attempting to align the probe above a flat plate with a reflective metallic surface, as illustrated in figure 8, to the test them. An alignment laser was used to define the optical axis of the setup and hence enabled correct positioning of the lenses with respect to the model; hot-wire probe and the LED back illuminating light source.
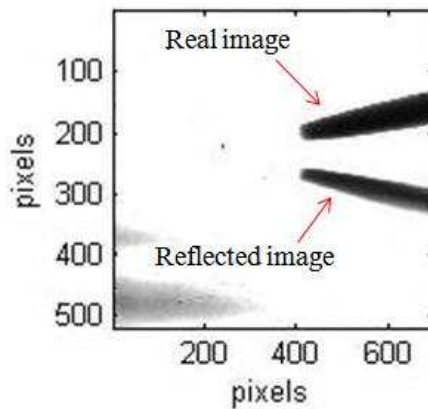

Figure 9: The real and reflected image of the probe captured using the CCD camera during the alignment on the flat plate.
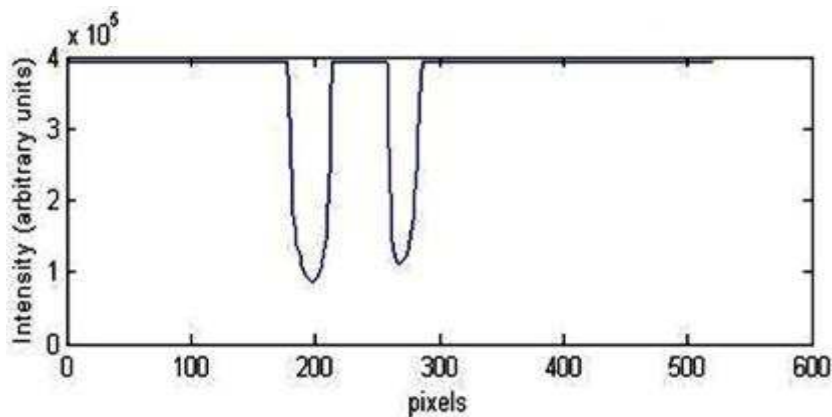

Figure 10: Colour intensity trace of the real and reflected image along the axis touching the tips of the hot wire support.

Due to the reflective nature of the surface, both the real image of the side of the hot-wire probe support and its mirror image could be captured by the CCD camera, as shown in figure 9. Again, through the digitisation process, the variation of the greyscale intensity along a vertical axis touching the tip of the hot wire support on both images could be plotted. In figure 10 the troughs represent the tips of the hot wire supports: the number of pixels between the end of the first trough and beginning of the second one show the separation between the two

images. Using factors obtained during the calibration process, the spacing between the tip of the hot wire support and the surface of the flat plate was calculated to be $163 \pm 0.14 \mu m$ with the tunnel operating at 20 m/s, assuming an error of 4 pixels from real and reflected image during digitisation. With the tunnel operating between 25-40m/s, no significant vibration was observed and the probe did not displace from its initial position, except at speed greater than 45m/s where the entire test section started to vibrate slightly and the whole image captured from the CCD sensor appeared to be moving on the screen.

Near-wall alignment of the probe for the swept wing model was more complicated due to the non-reflective nature of the wooden surface. Also, due to the relatively large distance between the object plane and optics which led to a two stage magnification, the optical aberrations from the curved surface became more severe and the resultant optical system did not yield reasonable image quality. An example of the resulting images of the side view of the hot-wire supports, at two different locations with respect to the model's surface, are shown in figure11. From the left-hand image, the hot wire appears to be in contact with the surface but in fact this was not the case. Whereas, for the right-hand image, the support was just in contact with the surface, but the image suggests that it was past the point of contact and had started to bend against the surface of the model. However, despite the poor image quality, once again no significant displacement of the probe was observed under the effect of wind loading. Therefore, the possibility of wind-off alignment was considered and the optical system was modified, so that the target was magnified only through a single magnification phase (similar to the set-up used for the calibration of the traverse mechanism) by placing the optical system inside the working section for wind-off alignment. This meant that the optical bed had to be shifted inside the test section as shown in figure 12, closer to the probe and the model surface, using a coarser traverse mechanism to move the lens mounted on the optical bed horizontally, closer to the target.

Figure 11: The blurred image of the side view of the hot wire probe support and the LE of the wind tunnel model obtained from the optical set-up placed outside the working section for wind on measurements.

Figure 13, obtained with the revised arrangement, shows an improved resolution of the contact between the wire supports and the wind tunnel model. Depending on the type of hot-wire probe and the angle through which it was driven towards the surface, there was a minimum separation between the sensor wire and the wall before the wire support, which was substantially thicker than the sensor wire, would come in contact with the wall and prohibit any further displacement. The minimum probe-to-wall distance achievable during the experiment was equal to the perpendicular distance between the centre of the hot wire and the tip of the support in contact with the wall. Using the method devised in section 2.4, this distance was determined to be approximately $60 \mu m$.

The near-wall positioning of the probe involved driving the probe, using the fine traverse mechanism introduced in section 2.2, towards the wall until contact was established. Further movements had to be minimised or else the wire supports would start to bend and damage the fragile sensor wire. This could also introduce lasting errors in the wall-normal distance. In addition to the digital display from the computer screen, another way of confirming whether contact was established with the surface was by operating the hot wire as a proximity sensor by monitoring the heat transfer between the hot wire and the wall. Using the real time signal display capability

in NI-Labview, the step change in the amplitude of the signal was monitored and as the wire was brought closer to the wall the increase in output voltage could be observed. Upon contact the largest step change in the signal was shown together with the maximum voltage output and stayed more or less constant for any further step motion of the traverse.
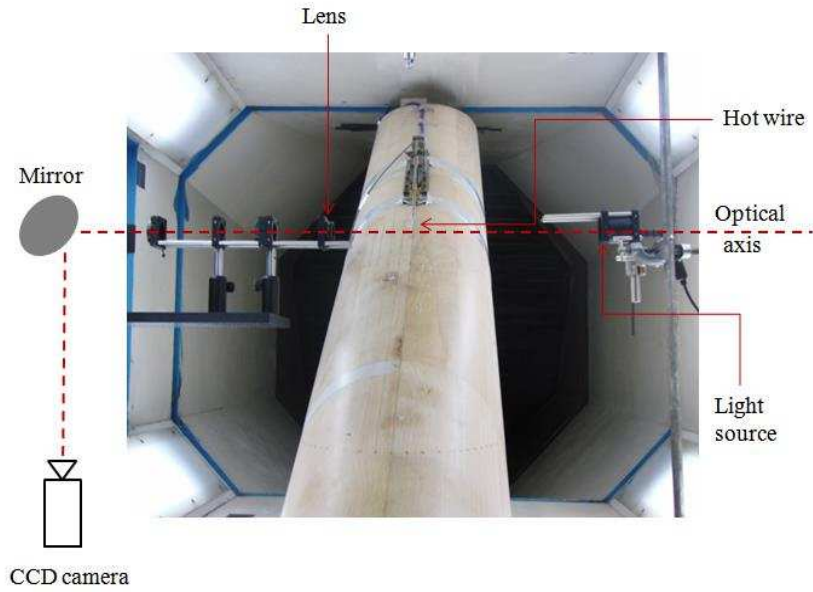

Figure 12: The modified optical set-up using a single lens for near wall positioning.
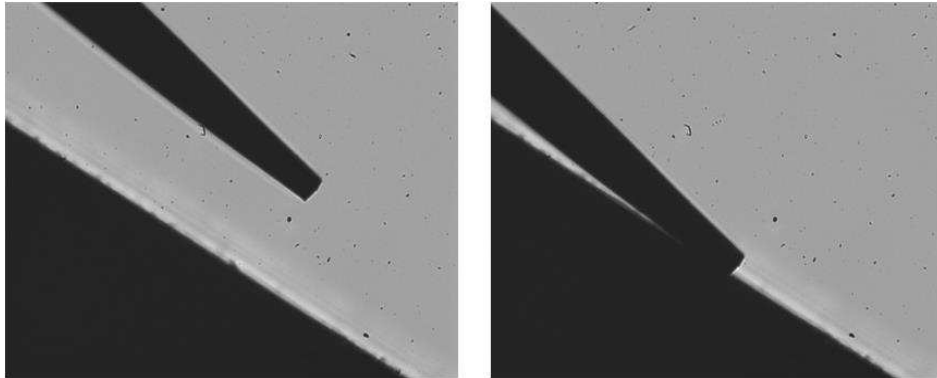

Figure 13: The side view of the probe support and the wind tunnel model obtained from the modified set-up placed positioned inside the working section.
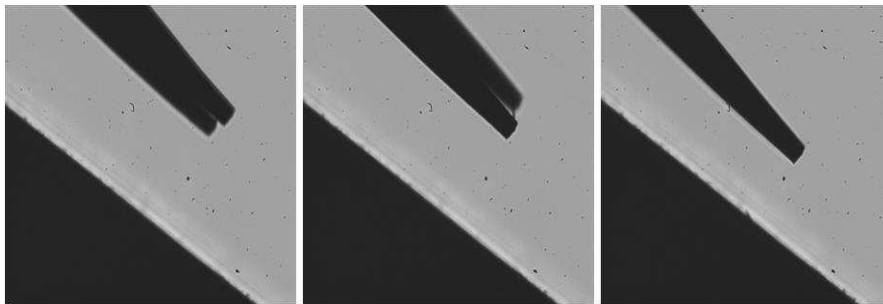

Figure 14: Aligning the wire supports.

When using this method the accuracy of the wall to probe position is highly dependent on the step resolution used while approaching the wall, in particular the measured position immediately before contact is established.

For the current experiment each step change was equal to a displacement of 4.82 μm. If, in the worst case scenario, this minimum probe height is half the displacement generated by the traverse, then the accuracy of the probe wall position is within $\pm 2.41 \mu$m. This can be further reduced by employing finer step changes, for example the quarter-step approach which would give an accuracy of $\pm 0.6 \mu$m for near-wall alignment. The optical system can also be employed to ensure that the wire supports are parallel to each other and are lying in the same plane. By comparing the three images presented in figure 14, it is clear that from the first two pictures the wire supports were not aligned in the same plane and they could be adjusted quite precisely simply by rotating the probe in its holder, as confirmed by the third picture.
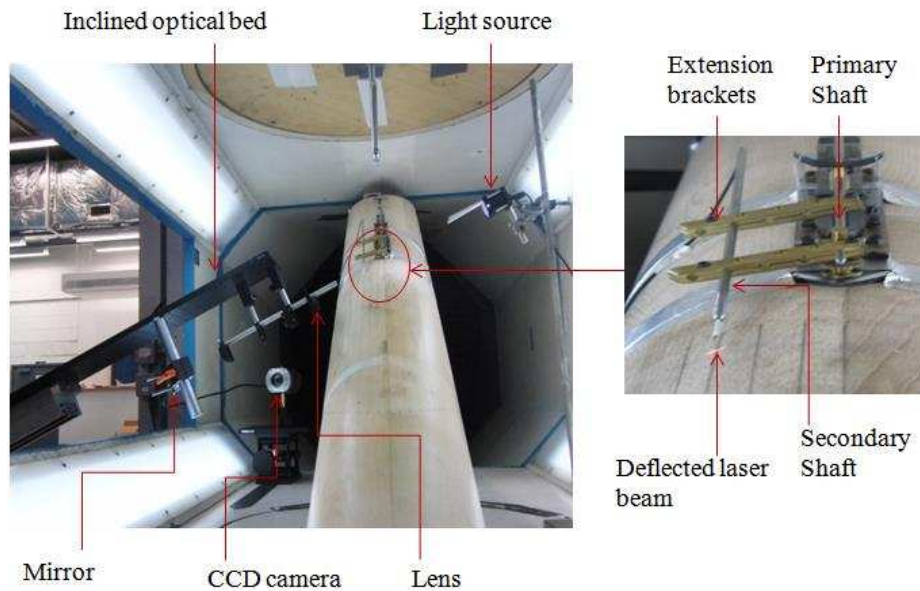

Figure 15: The set-up on an inclined optical bed for alignment along the highly curved surface downstream of the AL.
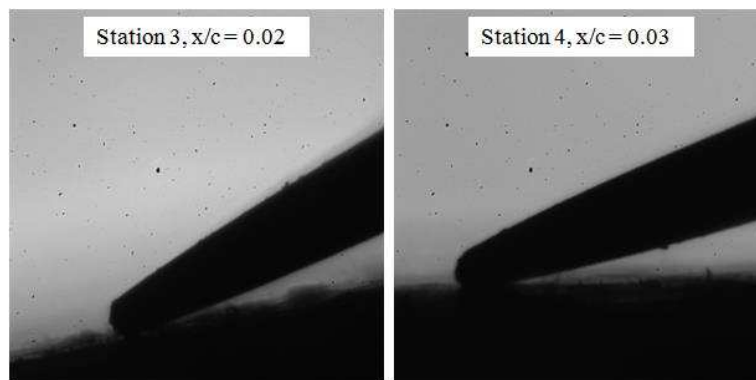

Figure 16: The side view of the probe support and the model surface for alignment downstream of the AL

For the measurements made downstream of the attachment line, of the optical bed (platform) was inclined about the horizontal axis using the adjustable angle plate on which it was mounted, but otherwise the optical method did not vary from the one used above. Again a laser beam was sent through the centre of the optics to define the optical axis, but this time tangential to a point away from the attachment line where the boundary layer measurement would be made. The tangent point could be identified by driving the laser beam towards the surface until the bottom part of the beam was in contact with the surface, causing the beam to deflect, creating a red spot labelled in figure 15 as 'Deflected laser beam'. The optimum tangential point was obtained by repeating this process until the spot size was minimised. After defining the optical axis, the laser emitter was replaced by the CCD camera and the image was brought into focus. The resulting images are shown in figure 16 for the alignment at 2 chordwise stations.

3.3. Velocity Profiles Measurements

The laminar velocity profiles captured are presented in figure 17 (where $\eta = z\sqrt{V_e/\nu r}$). Good agreement with both 'swept Hiemenz flow' theory, obtained from Rosenhead [15], and the measurements made by Gaster can be observed. However, very close to the surface the experimental result levels off at a velocity ratio of 0.1: this is indicative of heat transfer between the surface and the probe at low tunnel speed. According to Wills [1] this effect is minor or negligible for wooden surfaces or surfaces with poor heat conductivity; nevertheless, as the wire supports were in contact with the wall, heat transfer might have been significant. There are also some small discrepancies in the experimental results at velocity ratio less than 0.3 which may be the result of inaccurate low speed calibration, as the minimum speed achievable in the T2 tunnel is about 4 m/s.
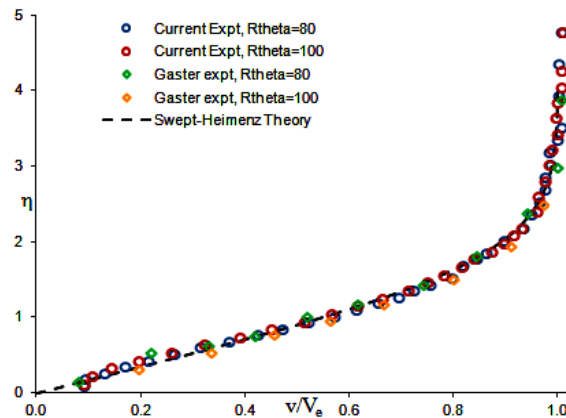

Figure 17: Comparing the laminar velocity profiles captured from the current experiment with the swept Hiemenz flow [15] and Gaster's [10] experiment.

As there are no published analytical solutions available for a turbulent AL boundary layer, and due to the scarcity of experimental data for this type of flow, the only comparison data available was the measurements made by Cumpsty and Head [11]. Figure 18 shows the turbulent velocity profiles captured during the current experiment (where $\zeta = z/\delta^*$) and they can be seen to agree well with the measurements made by Cumpsty and Head. Capturing the flow in the laminar sub-layer of a turbulent boundary layer is a very challenging exercise due to the very steep local velocity gradient in that region. The ability to capture smaller velocity ratios in comparison to Cumpsty and Head's measurements demonstrates the value of the optical set-up in aligning the hot-wire probe very close to the wall, coupled with the fine resolution of the traverse mechanism.
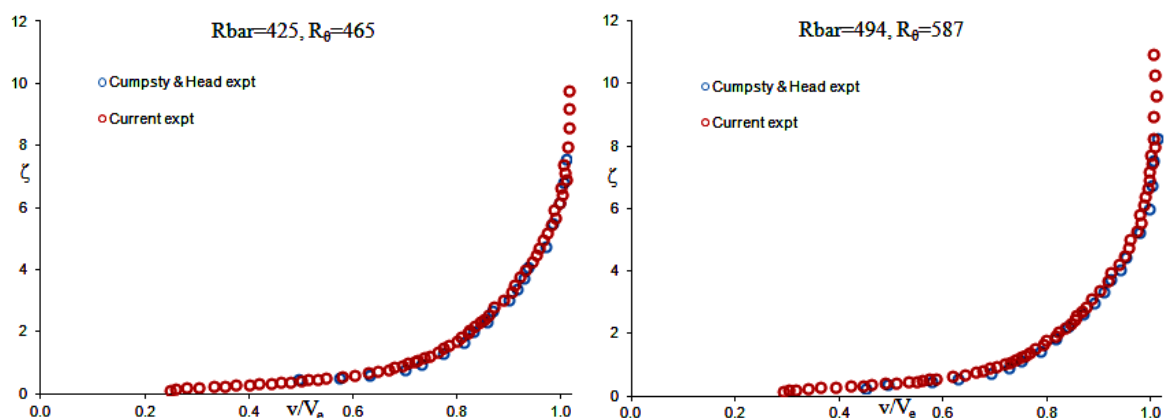

Figure 18: Velocity profiles of the turbulent AL captured experimentally by Cumpsty and Head's [11].

Using surface shear stress measurements obtained using Preston's technique (surface Pitot tube), the turbulent velocity profiles can be represented in wall units, as shown in figure 19. A good correlation can be observed with universal logarithmic law which represents the inner layer for $z^+ > 50$, unlike the results of Cumpsty and

Head, where a large scatter can be seen in "Figure 9" of reference [11]. Figure 19 shows that, for the lowest Reynolds number case, couple of measurements were obtained even in the laminar sub-layer, $z^+ < 5$, which is very difficult to resolve for a boundary layer approximately 3mm thick. Further displacement of the probe was impossible as the tips of the probe supports were already in contact with the surface; hence the lack of further data points in the laminar sub-layer. Modifications to the probe orientation will therefore be required for measurements even closer to the surface, provided that the heat transfer between the wall and the probe is negligible or correctable.
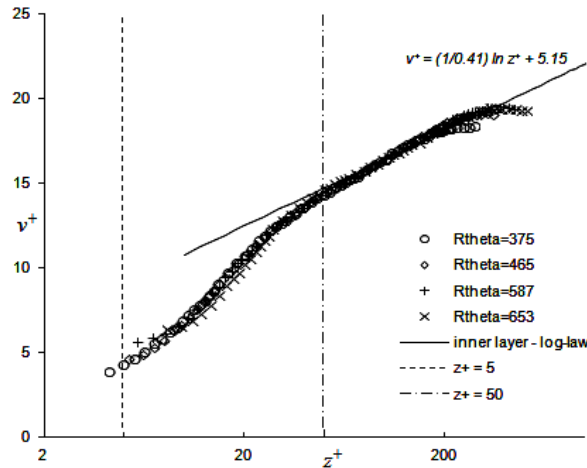

Figure 19: The turbulent AL velocity profiles represented in wall units.

From the velocity profile captured at the AL during the current experiment the momentum thickness, θ_{11}, was determined and is compared with those obtained by Cumpsty and Head in figure 20. The trend of variation with $\bar{R}$ is similar, but the absolute values obtained by Cumpsty and Head are lower than those from the current experimental results which is believed to be due to the higher resolution obtained during the current experiment. The better agreement of the current turbulent velocity profiles with the universal logarithmic law would suggest that the momentum thickness measured in the present experiment is more accurately captured.
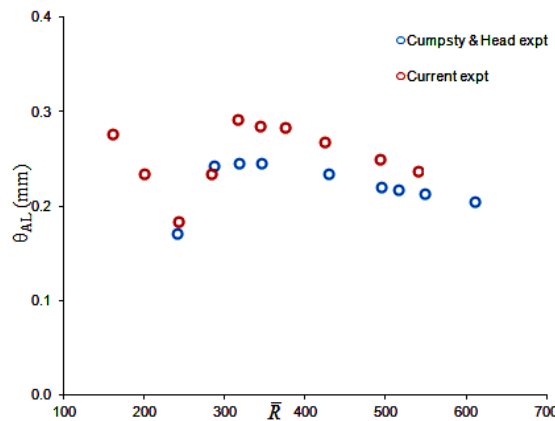

Figure 20: Variation of momentum thickness, θ with AL Reynolds number, $\bar{R}$

At freestream velocities above 30 m/s the temperature of the ambient freestream air inside the tunnel started to drift considerably: at the maximum speed of 55 m/s the temperature could rise by 15K, over a period of approximately half an hour. However, during the acquisition of all the data reported here the maximum temperature drift was usually below 10K. Still, the effect of thermal expansion of the traverse probe had to be considered. The main components that would contribute to most of the inaccuracy in this case are the tube which holds the probe and the wedge-slider, both made of steel. Based on the coefficient of thermal expansion coefficient of steel which is approximately $13 \times 10^{-6} \ K^{-1}$, for a set of measurements where a temperature rise

of 15K is encountered by the end of the run, the height of the wedge slider might increase by approximately 6μm, which is equivalent to less than 0.2% of the traverse height. This can be assumed to be negligible especially as it occurs during the traversing of the edge of the boundary layer where the step motions are significantly larger than the very fine initial displacements near the wall. On the other hand, for a similar temperature rise the maximum increment in the probe holder length, measured from the tip of the pivot, is approximately 15μm at the end of the traverse. The maximum pitch angle of the probe support with respect to the wall, which is normally at the initial measurement position, is approximately 8º and at the end of the traverse it is more or less parallel to the wall, as shown in figure 13. Due to the negligible pitch angle at the end of the measurement, the error in traverse height will be minimal; at the beginning of the measurement the temperature rise is not significant and pitch angle is still small as well (< 10º). This small pitch angle also suggests that the response of the hot wire to the wall-normal velocity component can be neglected compared to the in-plane velocity components.

4. Conclusions

A novel digital optical system was used to commission and test a traverse mechanism with very fine micro-displacement, and also to facilitate near wall alignment of a hot wire probe. Near wall alignment was easier on a reflective flat surface, such as an aluminium plate, and the optics could be kept outside of the wind tunnel, thus allowing for wind-on assessment of the traverse performance. However due to significant optical distortions near the curved surface of a swept wing the optics had to be placed inside the test section allowing wind-off alignment only. As no significant displacement of the probe was observed during the wind-on alignment on the flat plate, the discrepancies due to probe displacement through aerodynamic loading were also assumed to be negligible for measurements on the swept wing model. In the absence of significant probe displacement, and assuming accurate wind-off alignment, the system also enabled probe alignment along the highly curved surface at the leading edge of the wing which is usually an issue for such measurements. Measurements away from the leading edge were achieved by tilting the optical bed, while ensuring that the optical axis was tangential to the point measurement. As the wire sensor was located in the centre of the probe supports, there was a limit on the minimum achievable probe height; nevertheless this issue may be resolved by mounting the wire at the bottom of the supports rather than the middle, or simply by changing the probe orientation.

Comparison of the results obtained with the work of others suggests that the ability to capture accurately the profile very close to the wall, and the ability to fit in a large number of measurements, are important for measuring boundary layer properties such as the momentum or the displacement thickness, especially for a turbulent boundary layer. The ability to resolve the flow very near to the wall, and even within the laminar sub-layer for the lowest Reynolds number case, was attributed mainly to the precision of the traverse and the alignment system.

The accuracy of the alignment system was found to be better with only one magnification stage and without the use of the intermediate lens. Therefore the system is best suited to wind tunnel test sections of small cross-sectional area, as the optics can be placed outside the tunnel while still fulfilling the requirement for the focal length. Hence, this system will be ideal for small scale transonic or supersonic testing facilities, where the boundary layer is usually very thin. The system offers the additional capability to monitor the vibration of the probe in high speed flows.

5. Acknowledgement

6. References

[1]   Wills J A B 1962 The correction of to a hot-wire readings for proximity to a solid boundary J. Fluids Mech. **12**
[2]   Bruun H H 1995 Hot-wire anemometry - Principles and signal analysis Oxford University Press
[3]   Van Thinh N 1969 On some measurements made by means of a hot wire in a turbulent low near a wall DISA information

[4]   Krishnamoorthy L V Wood D H Antonia R A and Chambers A J 1985 Effect of wire diameter and overheat ratio near a conducting wall Exp. Fluids **3** 121

[5]   Devenport W J Evans G P and Sutton E P 1990 A traversing pulsed wire probe for velocity measurement near a wall Exp. Fluids **8** 336

[6]   Orlando A 1974 Turbulent transport of heat and momentum in a boundary layer subject to decceleration, suction and variable wall temperature PhD Thesis Stanford University

[7]   Hutchins N and Choi K S 2002 Accurate measurements of local skin friction coefficient using hot-wire anemometry Prog. Aero. Sci. **38** 412

[8]   Kerho M F 1995 Effect of large-disributed roughness near an aerofoil leading edge on boundary-layer development and transition PhD thesis University of Illinois

[9]   Takagi S 1985 Hot-wire height gaue using a laser and photodiodes Exp. Fluids **3** 341

[10]   Pfenninger W 1965 Flow Phenomena at the Leading Edge of Swept wings, Recent development in Boundary Layer Research AGARDograph **97**

[11]   Gaster M 1967 On the flow along swept leading edges Aeronautical Quarterly **17**

[12]   Poll D I A 1979 Transition in the infinite swept attachment line boundary layer Aeronautical Quarterly **30**

[13]   Cumpsty N A and Head M R 1969 The Calculation of the three-dimensional turbulent boundary layer Part III: Comparison of the attachment line calculations with experiment. Aeronautical Quarterly **20**

[14]   Atkin C J and Gowree E R 2013 On the experimental measurement of a turbulent Incompressible attachment line 48th International Symposium of Applied Aerodynamics

[15]   Rosenhead L 1963 Laminar Boundary Layers Oxford University Press

[16]   Atkin C J and Gowree E R 2012 Experimental investigation of the behaviour of incompressible turbulent attachment line and the flow in its proximity 47th International Symposium of Applied Aerodynamics

[17]   King L V 1914 On the convection of heat from small cylinders in a stream of fluid. Determination of convective constants of small platimium wires with application to hot-wire anemometry Phil. Trans. Roy. Soc. **214**

[18]   Collis D C and Williams M J 1959 Two-dimensional convection from heated wires at low Reynolds numbers J. Fluid Mech. **16**

[19]   Abdel-Rahman A., Tropea C, Slawson P. and Strong A 1987 On Temperature compensation in hot-wire anemometry J. Phys. E: Sci. Inst. **20**